

# Journal of Materials Chemistry B

Accepted Manuscript



This is an *Accepted Manuscript*, which has been through the RSC Publishing peer review process and has been accepted for publication.

*Accepted Manuscripts* are published online shortly after acceptance, which is prior to technical editing, formatting and proof reading. This free service from RSC Publishing allows authors to make their results available to the community, in citable form, before publication of the edited article. This *Accepted Manuscript* will be replaced by the edited and formatted *Advance Article* as soon as this is available.

To cite this manuscript please use its permanent Digital Object Identifier (DOI®), which is identical for all formats of publication.

More information about *Accepted Manuscripts* can be found in the [Information for Authors](#).

Please note that technical editing may introduce minor changes to the text and/or graphics contained in the manuscript submitted by the author(s) which may alter content, and that the standard [Terms & Conditions](#) and the [ethical guidelines](#) that apply to the journal are still applicable. In no event shall the RSC be held responsible for any errors or omissions in these *Accepted Manuscript* manuscripts or any consequences arising from the use of any information contained in them.

## ARTICLE

# Bioinspired assembly of layered double hydroxide/carboxymethyl chitosan bionanocomposite hydrogel films

Cite this: DOI: 10.1039/x0xx00000x

Yi Wang and Dun Zhang

Received 00th January 2012,

Accepted 00th January 2012

DOI: 10.1039/x0xx00000x

[www.rsc.org/](http://www.rsc.org/)

Carboxymethyl chitosan (CMC) intercalated Mg–Al layered double hydroxides (C-LDHs) with a high dispersion in the CMC matrix were successfully synthesised by a one-pot method using a facile biopolymer-assisted approach in the presence of CMC under hydrothermal conditions. Highly oriented, flexible and glossy self-supporting C-LDH/CMC bionanocomposite hydrogel films with good mechanical properties were bioinspired assembled using C-LDH nanoplatelets and CMC molecules as building blocks via the solvent evaporation process. The results of X-ray diffraction and scanning electron microscopy showed that the bionanocomposite film had a bioinspired layered structure. The film thickness and equilibrium swelling ratio of the C-LDH/CMC bionanocomposite film could be changed by adjusting the C-LDH mass content. The film with a high C-LDH mass content had a high swelling stability, which may be attributed to the LDH nanoplatelets that could act as crosslinkers to reinforce the bionanocomposite film structure. Lysozyme could be immobilised in the C-LDH/CMC bionanocomposite hydrogel film through electrostatic interaction.

## Introduction

Over the last few years, studies in materials science have focused on bionanocomposites with extraordinary multifunctional properties by combining various natural occurring biopolymers and inorganic solids together into a well-designed structure.<sup>1</sup> Chitosan (CS) and layered double hydroxides (LDHs) are two of the most powerful materials that are widely used as essential elements for fabricating novel artificial bionanocomposites, especially for recreating a bioinspired layered “brick-and-mortar” structure.<sup>2–4</sup> CS is a linear cationic amino polysaccharide and is the second most abundant natural polysaccharide present on earth next to cellulose.<sup>5</sup> LDHs are a family of synthetic anionic clays composed of 2D brucite Mg(OH)<sub>2</sub>-like layered inorganic materials. They are expressed by a general formula  $[M^{2+}_x M^{3+}_x(OH)_2]A^{n-}_{x/n} mH_2O$ , where M<sup>2+</sup> and M<sup>3+</sup> are divalent and trivalent metal ions coordinated octahedrally by hydroxyl groups to form infinite 2D layers by edge sharing and the A<sup>n-</sup> anion is the interlayer anion compensating for the positive charge of the brucite-like layers.<sup>6,7</sup> Different from naturally occurring anionic clays, such as montmorillonite (MMT), cationic LDHs can serve as catalytic, functional, biological, and medical materials because of their tunable compositions and exchangeable anions.<sup>8</sup> Therefore, using LDH as a building

block for fabricating bioinspired bionanocomposite films will achieve not only high strength but also other special functionalities.<sup>2</sup>

Different techniques, such as layer-by-layer assembly,<sup>9, 10</sup> ice-crystal template,<sup>11, 12</sup> paper making,<sup>13</sup> dip coating<sup>2</sup> and solvent evaporation,<sup>3</sup> have been recently explored to fabricate bionanocomposite films. Among these techniques, solvent evaporation has received considerable attention because it is cheap, simple, fast, time saving, environmentally friendly, and easily scaled up. Well dispersion of inorganic LDH phase in the CS matrix is needed to obtain an LDH/CS bionanocomposite film with a high mechanical property using this route.<sup>3</sup> The intercalation of CS into LDHs is an efficient strategy to solve this problem.<sup>14, 15</sup> Several anionic biopolymers, such as DNA<sup>16</sup> and naturally occurring polysaccharides, including alginic acid, pectin and *t*-carrageenan,<sup>17</sup> are reported to be intercalated into the LDH interlayer; however, CS intercalation is seldom reported because of its low solubility in alkaline medium and positively charged nature.<sup>5</sup> Moreover, the reported biopolymer intercalated LDH bionanocomposites are mostly particles that cannot be well dispersed in the biopolymer matrix, which is not facile for the preparation of bionanocomposite films via solvent evaporation. This phenomenon encouraged us to further challenge the goal of fabricating CS intercalated LDHs that can be well dispersed in the CS matrix.

Carboxymethyl CS (CMC) is an important CS derivative extensively used in a wide range of biomedical applications because of its good water solubility, unique chemical, physical and biological properties and excellent biocompatibility and biodegradability.<sup>18–24</sup> A large number of carboxyl groups and amide groups within the skeletal framework of CMC can interact with chelating metal cations in alkaline medium.<sup>25</sup> Thus, CMC may act as an organic template to induce the formation of special nanostructural materials.<sup>26</sup> In addition, as an anionic biopolymer, CMC may be intercalated into the LDH interlayer as a guest molecule.

This study introduces a two-step approach to fabricate LDH/CMC bionanocomposite films. Firstly, CMC intercalated Mg–Al LDHs (C-LDHs) were synthesised by the hydrothermal method, and the obtained C-LDHs were well dispersed in the CMC matrix to form a stable colloidal suspension. Then, a transparent, flexible and glossy self-supporting film with a highly oriented lamellar microstructure was easily bioinspired assembled during the solvent evaporation process. This bionanocomposite film with a high swelling ratio and stability had a high mechanical property and was used to immobilise lysozyme (LSZ). This strategy is an alternative approach to fabricate LDH/CMC bionanocomposite hydrogel films, which can be potentially used in the field of enzyme immobilisation, underwater antibacterial coating, drug storage and delivery, biosystem, etc.

## Experimental

### Materials

CMC with a substitution degree of 0.92 and a molecular weight of 9000 was purchased from Jinan Haohua Industry Co., Ltd. (China). Other analytical reagent-grade chemicals were supplied by Sinopharm Chemical Reagent Co., Ltd. Milli-Q water was used in the experiments (Millipore, USA).

### C-LDH synthesis

In a typical synthesis, urea,  $\text{Mg}(\text{NO}_3)_2 \cdot 6\text{H}_2\text{O}$  and  $\text{Al}(\text{NO}_3)_3 \cdot 9\text{H}_2\text{O}$  with a Mg/Al molar ratio of 2.0 and a urea/metal cation ratio of 3.3 were dissolved in 40 mL of water to obtain a clear solution with metal cation concentrations of 0.12, 0.060, 0.030 and 0.015 M. A total of 40 mL of this mixture solution was added into 40 mL of CMC solution with a concentration of 1 g/L under stirring condition. The mixture was then transferred in an autoclave and heated at 100 °C for 24 h. According to the P–T diagram of pure water with various initial filling degrees, the estimated pressure was 0.02 GPa.<sup>27</sup> The resulting suspension was ultrasonicated for 3 h and then centrifuged at 4000 r/min for 20 min. Finally, a very stable milky white suspension was obtained without visible precipitation after storage for several months.

### Preparation of C-LDH/CMC bionanocomposite hydrogel films

The obtained colloidal suspension (10 mL) was dropped into a PTFE module, placed in an oven at 40 °C and then completely

dried. A transparent, flexible and glossy self-supporting bionanocomposite film was easily peeled off for further study. The final obtained C-LDH/CMC bionanocomposite films with different C-LDH/CMC mass ratios were denoted as LC-1, LC-2, LC-3 and LC-4, which corresponded to the C-LDH mass contents of 72%, 47%, 29% and 23% after calculation, respectively. For comparison, pure CMC film without C-LDHs and any crosslinkers was fabricated via the same route.

### Characterisation

X-ray diffraction (XRD) measurement was performed on a D/MAX 2250 V diffractometer (Rigaku, Japan) using monochromatised  $\text{Cu K}\alpha$  radiation ( $\lambda = 1.54178 \text{ \AA}$ ) with  $2\theta$  ranging from 3° to 70°. Fourier transform infrared (FT-IR) spectra were collected on a Nicolet iS10 infrared spectrophotometer (USA) using KBr disks with a sample/KBr mass ratio of 1:100. Zeta potential measurement was carried out using a Malvern Zetasizer Nano (England) at room temperature. Transmission electron microscopic (TEM) observations were performed under a JEOL 1200 transmission electron microscope (Japan) at an accelerating voltage of 100 kV. Scanning electron microscopy (SEM) images were observed under a Hitachi S-4800 SEM (Japan). The samples were also subjected to energy-dispersive X-ray spectroscopy (EDS) during the SEM measurement. The mechanical properties of the self-supporting films were measured under tensile mode in a WDW-100E universal mechanical testing machine (China). For the mechanical tests, the films were cut into rectangular bars of approximately 20 mm in length and 10 mm in width with a razor blade. The distances between the clamps and the load speed were 5 mm and 1 mm/min, respectively.

### Swelling characteristics of C-LDH/CMC bionanocomposite hydrogel films

The obtained C-LDH/CMC bionanocomposite films with different C-LDH mass contents were immersed in 20 mL of water at room temperature until swelling equilibrium was attained. The swelling ratio of the bionanocomposite film was calculated from the following expression:<sup>19</sup>

$$\text{Swelling ratio} = ((W_t - W_d) / W_d) \times 100\% \quad (1)$$

where  $W_d$  is the weight of the dry film and  $W_t$  is the weight of the wet film at the equilibrium swelling state.

### Immobilisation of LSZ by C-LDH/CMC bionanocomposite hydrogel films

The C-LDH/CMC bionanocomposite films with different C-LDH mass contents were immersed in 10 mL of LSZ solution (1 mg/mL) at room temperature for 24 h. Then, the hydrogel film was taken out, dried and reweighed. The amount of LSZ solution left in the loading medium was determined by measuring the absorbance value at 282 nm using a Hitachi U2900 UV–Vis spectrophotometer (Japan) to confirm the percentage of LSZ immobilisation in hydrogel films.

## Results and discussion

Fig. 1 shows the XRD patterns of the pure CMC film as well as the synthesised C-LDH/CMC bionanocomposite hydrogel films with different C-LDH mass contents. The pattern of the C-LDH/CMC bionanocomposite film was composed of characteristic reflections of C-LDHs and CMC. Moreover, in each case, the C-LDH sample presented hydrotalcite-like characteristic reflections of (003), (006) and (009) peaks at low angle, and  $d_{003}$ ,  $d_{006}$  and  $d_{009}$  showed the expected relationship between basal, second-order and third-order reflections.<sup>28</sup> In addition, the absence of any non-basal reflections ( $h, k \neq 0$ ) at high angle indicated that the bionanocomposite hydrogel film had an extremely well  $c$ -oriented assembly of LDH nanoplatelets.<sup>29</sup> The interlayer spacing ( $l$ ) was calculated by averaging the positions of three harmonics:  $l = (1/3)(d_{003} + 2d_{006} + 3d_{009})$ .<sup>28</sup> The calculated interlayer spacings for LC-1, LC-2, LC-3 and LC-4 were 1.15, 1.20, 1.16 and 1.21 nm, respectively. By subtracting the thickness of the LDH layer (0.48 nm),<sup>28</sup> the gallery heights of 0.67, 0.72, 0.68 and 0.73 nm for LC-1, LC-2, LC-3 and LC-4, respectively, could be obtained. These values indicated that the CMC molecules were intercalated in a monolayer arrangement.<sup>17</sup>

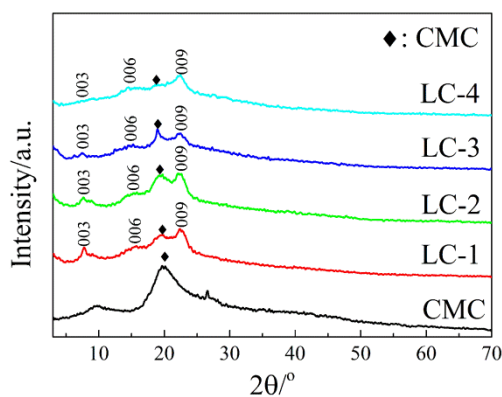


Fig. 1 XRD patterns of the pure CMC film and the C-LDH/CMC bionanocomposite films with different C-LDH mass contents

FT-IR spectra provided another evidence for the formation of C-LDH/CMC bionanocomposite hydrogel films (Figs. 2 and 1S in the ESI). For the spectrum of the pure CMC film, the bands at 1069 and 1159  $\text{cm}^{-1}$  were attributed to the C–O stretching vibration of –CH–OH in cyclic alcohols and C–O–C in ethers, respectively.<sup>19</sup> The band at 1413  $\text{cm}^{-1}$  was attributed to the stretching vibration of the –COO<sup>−</sup> group of carboxymethyl in the CMC,<sup>30</sup> and the bands at 1560 and 1655  $\text{cm}^{-1}$  were assigned to the C=O stretching vibration of carboxymethyl groups overlapped with amide N–H bending.<sup>31</sup> A broad band between 3100 and 3700  $\text{cm}^{-1}$  centred at 3439  $\text{cm}^{-1}$  was assigned to the stretching vibration of the O–H group and the extension vibration of the N–H group.<sup>32</sup> For the spectra of the C-LDH/CMC bionanocomposite film with different C-LDH mass contents, a broad band between 3100 and 3700  $\text{cm}^{-1}$  was attributed to the O–H and N–H stretching vibration. Hydroxyl

groups belonged to brucite layers and water overlapped with the O–H and N–H vibration of CMC.<sup>17</sup> The new band at 1628  $\text{cm}^{-1}$  was attributed to the H–O–H vibration of water molecules. The band location at 1655  $\text{cm}^{-1}$  and the band intensity at 1560  $\text{cm}^{-1}$  changed after composition. These results indicated a strong hydrogen bonding between the N–H groups of the CMC and hydroxyl of the LDH brucite layer. As shown in Fig. 2, the band at 1413  $\text{cm}^{-1}$  shifted toward a lower wavenumber when the CMC was incorporated with the LDH lamellae. This result indicated a strong interaction of the negatively charged group (–COO<sup>−</sup>) of the CMC with the positively charged LDH brucite layers. Absorption bands at approximately 593, 529 and 420  $\text{cm}^{-1}$  were attributed to the vibration of M–O and O–M–O in the LDH brucite layer, indicating that the LDH structure was formed when the CMC was intercalated between the layers, as confirmed previously by XRD.<sup>17</sup> The band intensity at 1159  $\text{cm}^{-1}$  did not change, suggesting that no depolymerisation occurred during the hydrothermal treatment.<sup>32</sup>

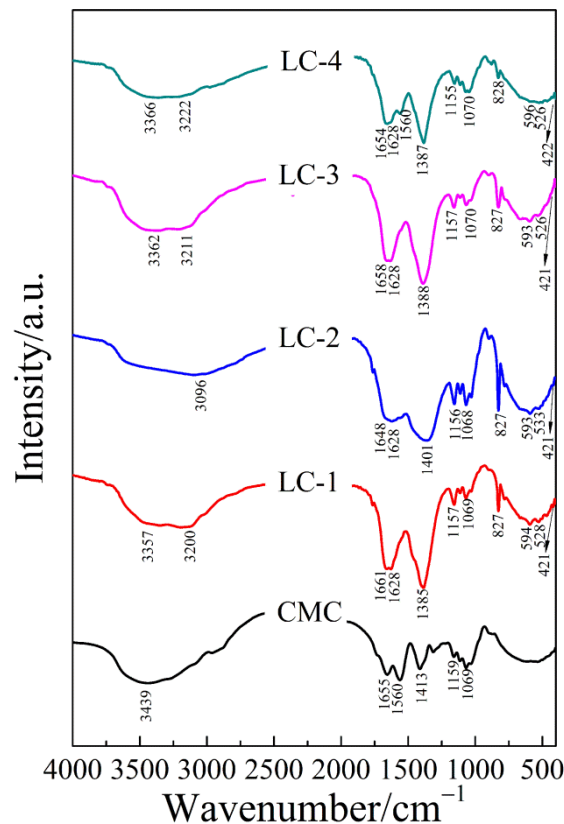
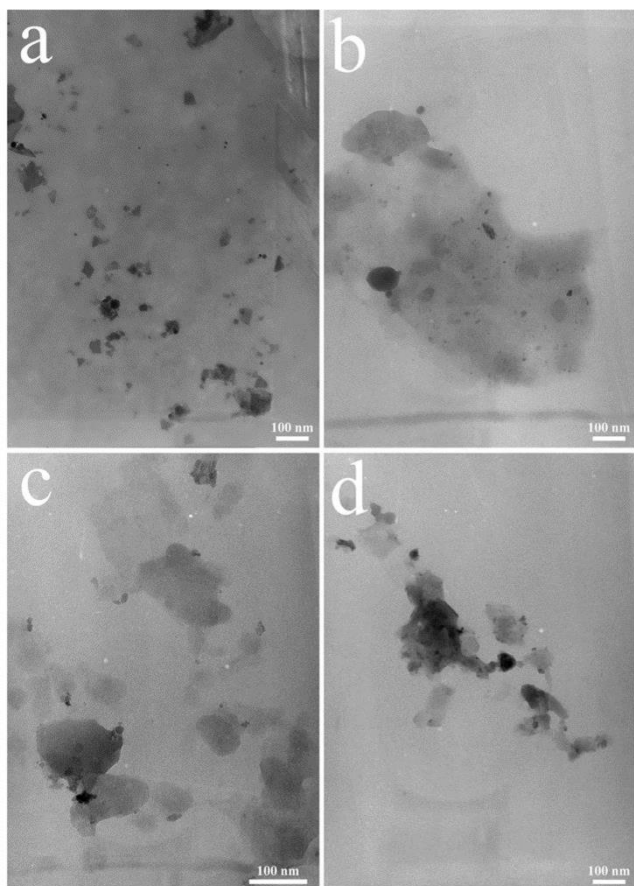


Fig. 2 FT-IR spectra of the pure CMC film and the C-LDH/CMC bionanocomposite films with different C-LDH mass contents

TEM images showed that the four synthesised C-LDH/CMC bionanocomposites with different C-LDHs mass contents had similar morphologies and consisted of irregular and thin hexagonal nanoplatelets with a particle size distribution ranging from 20 nm to 70 nm (Fig. 3). A typical HRTEM image of an

individual C-LDH nanoplatelet for the LC-1 sample (Figs. 4a and 4b) reveals the presence of an interplanar distance of approximately 0.264 nm, which is a characteristic of the (120) plane.<sup>33</sup> This distance confirmed the formation of LDH phase. The side view of HRTEM image (Fig. 4c) shows that the thickness of the C-LDH nanoplatelet was approximately 20 nm, indicating that approximately 17 monolayers stacked in the *c* direction.



**Fig. 3** TEM images of the C-LDH/CMC bionanocomposites with different C-LDH mass contents (a: LC-1; b: LC-2; c: LC-3; d: LC-4)

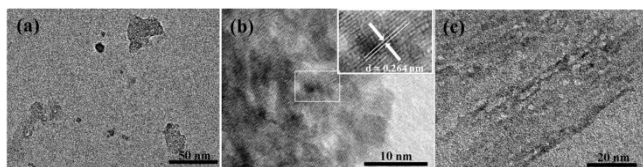


**Fig. 4** HRTEM images of the LC-1 sample (a and b: top view; c: side view)

The thickness and surface morphology of the four synthesised C-LDH/CMC bionanocomposite films with different C-LDH mass contents were further investigated by SEM (Fig. 5). Fig. 5b shows that C-LDH/CMC bionanocomposites were stacked together to form a densely oriented lamellar microstructure, which is reminiscent of the brick-and-mortar structure of nacre.<sup>3, 9, 13</sup> This result is consistent with the XRD result and indicates the occurrence of

the bioinspired assembly process.<sup>1, 2, 4, 34</sup> The top view of the SEM image shows that the obtained LC-1, LC-3 and LC-4 samples had a similar homogeneous surface with nanoscale roughness (Figs. 5a, 5e and 5g). Compared with these samples, the LC-2 sample had a slightly more rough surface (Fig. 5c), which may be attributed to the different CMC contents in the biocomposite film. These results indicated that both high inorganic C-LDH nanoplatelet content and high organic CMC content were facile to the formation of smooth surface. Moreover, the film thickness increased with decreasing C-LDH mass content (Figs. 5b, 5d, 5f and 5h). This finding indicated that the film thickness could be easily changed by adjusting the film composition.

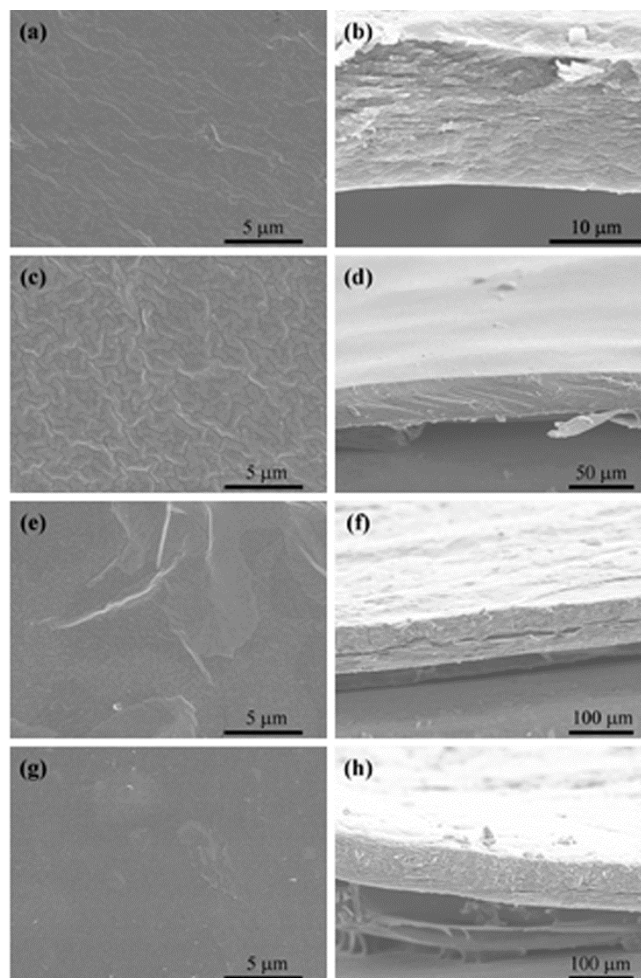
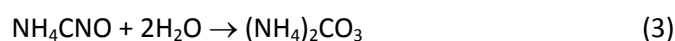


**Fig. 5** SEM images in top view (a, c, e and g) and cross-sectional view (b, d, f and h) of the C-LDH/CMC bionanocomposite films with different C-LDH mass contents (a and b: LC-1; c and d: LC-2; e and f: LC-3; g and h: LC-4)

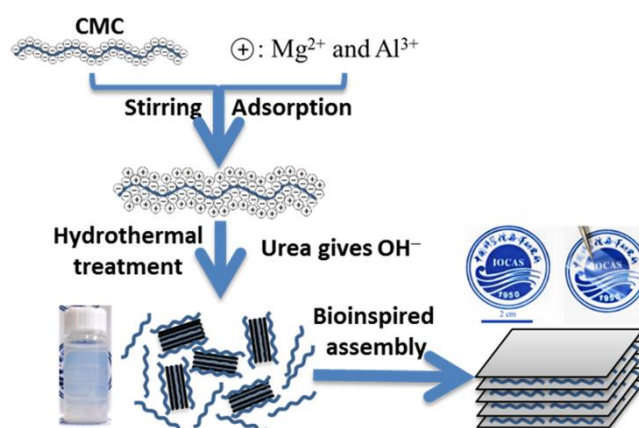
A schematic illustration of the formation mechanism of the bioinspired assembled bionanocomposite hydrogel film with CMC assistance is shown in Scheme 1. CMC is among the derivatives of CS. It is an amphiprotic ether that contains hydroxyl, carboxyl and amine groups in the molecule, which possibly offer enough chelate groups to increase adsorption capacity toward the metal ion.<sup>35</sup> The saturated adsorption

capacity of the CMC for  $Mg^{2+}$  and  $Al^{3+}$  ions can reach up to 106<sup>36</sup> and 250 mg/g,<sup>37</sup> respectively. Thus, the CMC molecule can be used as a biomineralisation template to modify the Mg–Al LDH growth.<sup>38</sup> Hydrothermal treatment combined with urea hydrolysis is a facile approach of co-precipitating  $Mg^{2+}$  and  $Al^{3+}$  ions to uniform and high crystalline Mg–Al LDHs with a controlled size and morphology.<sup>39–41</sup> Urea is a very weak Brønsted base ( $pK_b = 13.8$ ) that is highly soluble in water. The hydrolysis rate of urea can be easily controlled by controlling the reaction temperature. According to Shaw and Bordeaux,<sup>42</sup> the mechanism of urea hydrolysis consists of the formation of ammonium cyanate ( $NH_4CNO$ ), as the rate determining step, and the fast hydrolysis of the cyanate to ammonium carbonate, i.e.,



The rate constant increased by approximately 200 times when the temperature was increased from 60 °C to 100 °C. The hydrolysis of ammonium to ammonia and carbonate to hydrogen carbonates increases the pH value.<sup>42</sup> Fig. S2 (shown in the ESI) shows the pH evolution during the hydrothermal reaction within the initial 10 h. The two steps of pH variation were observed: at the earlier stage ( $t < 2$  h), the pH increased from 7 to 9 and then reached a plateau. The final pH (24 h) of the reaction solution was 9.02, which is a suitable value for co-precipitating Mg–Al LDHs.<sup>40</sup> During the first step at low pH conditions,  $OH^-$  anions produced by urea hydrolysis could react immediately with  $Al^{3+}$  cation to induce the precipitation of  $Al(OH)_3$ . At these pH values, the  $Mg^{2+}$  cation could not be co-precipitated with  $Al^{3+}$  cation. In the second step, the rate of  $OH^-$  consumption was faster than its production by urea hydrolysis, and the pH varied very slowly. This condition produced a very low  $OH^-$  supersaturation level. During this period,  $Mg^{2+}$  cation was incorporated in the solid hydroxide probably under a dissolution/precipitation mechanism.<sup>40</sup> Finally, Mg–Al LDH layer formed along the CMC chain. The obtained colloidal suspension was milky white and stable without precipitation after storage for several months, indicating that the synthesised C-LDH nanoplatelets had a good dispersal in the CMC matrix. Given the permanent positive surface charge of the particles arising from ion substitutions in the sheets, LDH had a positively charged surface.<sup>43</sup> However, the Zeta potentials of the four synthesised colloidal suspensions with different C-LDH mass contents were  $-2.27$ ,  $-4.61$ ,  $-3.38$  and  $-3.21$  mV, respectively. This result indicated that the free negatively charged CMC molecules in the solution could be adsorbed on the positively charged surface of C-LDH nanoplatelets to form C-LDH/CMC bionanocomposite materials, as reported extensively in studies of polymers adsorbing at solid/liquid interfaces.<sup>44</sup> Such adsorption may occur via the hydrogen bonding between the hydroxyl of the LDH brucite layers and amide groups of the CMC molecules, which was previously confirmed by the FT-IR result and the

electrostatic interaction between the negatively charged CMC molecules and positively charged LDH nanoplatelets.<sup>45</sup> The presence of the CMC shell renders the LDH nanoplatelet water soluble and leads to a steric stabilising effect by isolating the bionanocomposite from each other.<sup>21</sup> This resulting monodisperse colloidal suspension of C-LDH nanoplatelets is an ideal precursor for the fabrication of highly oriented self-supporting C-LDH/CMC bionanocomposite film via solvent evaporation.<sup>29</sup> Photographs of the obtained C-LDH/CMC bionanocomposite hydrogel films are shown in Scheme 1. These films are transparent, flexible and glossy.



**Scheme 1** Schematic of the bioinspired assembly process for the fabrication of C-LDH/CMC bionanocomposite film

**Table 1** Mechanical properties of C-LDH/CMC bionanocomposite hydrogel films with different C-LDH mass contents measured by tensile testing

| Sample | Tensile strength/MPa | Ultimate strain/% |
|--------|----------------------|-------------------|
| LC-1   | 34.65                | 8.40              |
| LC-2   | 21.48                | 11.20             |
| LC-3   | 13.52                | 13.92             |
| LC-4   | 12.07                | 17.16             |
| CMC    | 5.12                 | 21.16             |

The mechanical properties of the obtained bionanocomposite hydrogel films are summarised in Table 1 according to the tensile strength–strain curves (Fig. S3 in the ESI). The mechanical performance of the bionanocomposite hydrogel film was better than that of the pure CMC film. The tensile strength increased and the ultimate strain decreased as the C-LDH content increased from 23% to 72%. The tensile strength of the LC-1 sample was approximately sevenfold higher than that of the pure CMC film. This strength can be attributed to the strong hydrogen bonding and electrostatic interaction between the CMC molecules and the LDH brucite layers. In this study, LDH nanoplatelets were uniformly dispersed in the CMC matrix, which led to a narrow distribution of distance between LDH nanoplatelets.<sup>13</sup> The well-dispersed LDH nanoplatelets acting as crosslinkers were linked by flexible CMC molecules, which is consistent with a previous report on the CS/MMT composite film.<sup>3</sup> Consequently, the C-LDH/CMC bionanocomposite hydrogel films synergistically combined the stiffness of inorganic LDHs with the flexibility of organic CMC and showed enhanced mechanical properties.

The obtained C-LDH/CMC bionanocomposite films were allowed to swell in water at room temperature. None of the C-LDH/CMC bionanocomposite films dissolved when stored in water for several months, which can be attributed to the unique C-LDH/CMC network structure.<sup>3, 13</sup> By contrast, the pure CMC film without any crosslinkers dissolved immediately when immersed in water. The effects of the C-LDH content on the swelling ratio are shown in Fig. 6a. The swelling ratio increased with decreasing C-LDH mass content. At a low C-LDH loading level (LC-4), the swelling ratio reached 1370%, which is similar to that of genipin cross-linked CMC hydrogel (1100% to 1500%, pH 7.4).<sup>19, 46</sup> At a high C-LDH loading level (LC-1), the swelling ratio of 130% was still higher than that of glutaraldehyde-cross-linked CMC hydrogel (70% to 100%, pH 7.4).<sup>18, 30</sup> These results showed that the C-LDH nanoplatelets with good biocompatibility and similar crosslinking capacity like the natural occurring green crosslinker genipin may be an alternative selection as an environmentally friendly crosslinker for the CMC-based hydrogel film. The variation in the swelling ratio with the change in the C-LDH content can be attributed to the fact that an increase in the C-LDH nanoplatelet mass content can increase the crosslinking degree of the bionanocomposite film. This phenomenon is one of the most essential factors that affect the water absorption of hydrogel.<sup>47</sup> Compared with the swelling ratio, the swelling stability of bionanocomposite films increased as the C-LDH mass content increased (Fig. 6b). After 10 dry/wet cycles, the swelling ratio of the LC-1 sample with a high C-LDH mass content only decreased by approximately 10%, whereas that of the LC-4 sample with a low C-LDH mass content decreased by 25%. These results showed that this bionanocomposite film with a high C-LDH content can be reused many times, which can enlarge the application field and save sources. Consequently, inorganic LDH layer can be used as an alternative green crosslinker for the preparation of the CMC-based hydrogel film.

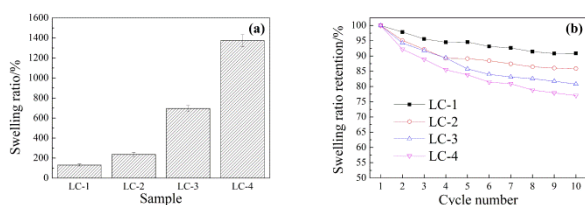


**Fig. 6** (a) Swelling ratio and (b) relationship between the swelling ratio retention and dry/wet cycle number of the C-LDH/CMC bionanocomposite films with different C-LDH mass contents

LSZ is a natural antibacterial protein that occurs in a wide range of animals and plants. The isoelectric point of LSZ is approximately 11, and LSZ is positively charged over the normal pH range. Thus, immobilisation by the C-LDH/CMC bionanocomposite hydrogel films is expected through electrostatic interaction.<sup>48</sup> LSZ immobilisation experiments were performed by immersing the obtained C-LDH/CMC bionanocomposite hydrogel films into LSZ solutions, and the results are shown in Fig. 7. The amount of LSZ immobilised in

the bionanocomposite hydrogel increased with decreasing C-LDH content, which is consistent with the swelling test result. These results can be attributed to the fact that bionanocomposite films with a high swelling ratio can provide more sites to immobilise LSZ during the swelling process.<sup>49</sup> Consequently, the C-LDH/CMC bionanocomposite hydrogel film would be a good platform for the immobilisation of positively charged enzyme at the neutral pH range.

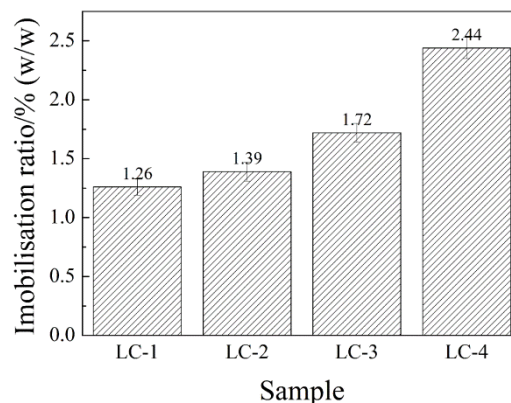


**Fig. 7** LSZ immobilisation ratio of the C-LDH/CMC bionanocomposite films with different C-LDH mass contents

## Conclusions

In summary, C-LDHs with a high dispersal in the CMC matrix were prepared by a one-pot hydrothermal method. The bioinspired assembly was used to fabricate free-standing and strong bionanocomposite films using C-LDH nanoplatelets and CMC molecules as building blocks via solvent evaporation. The characterisations via XRD, FT-IR, TEM, SEM and tensile testing indicated that the bionanocomposite film with a high mechanical property had a highly oriented bioinspired layered microstructure and that C-LDH nanoplatelets can act as crosslinkers to reinforce the bionanocomposite films. C-LDH/CMC bionanocomposite films with a high swelling ratio can maintain their self-supported shapes after 10 dry/wet cycles and can serve as an enzyme immobilising platform for the LSZ immobilisation. These findings provide an alternative route to fabricate LDH/biopolymer bionanocomposite films with multifunctionality for applications, such as biosensor, biomedical, enzyme immobilisation, artificial muscles, robust underwater antibiofouling materials and other environmentally friendly materials.

## Acknowledgements

This work was supported by Nature Science Foundation of China (Grant Nos. 21101160), Shandong Provincial Natural Science Foundation, China (Grant No. ZR2010BQ017), and Open Project Program of State Key Laboratory of Chemical Resource Engineering (CRE-2013-C-103).

## Notes and references

Key Laboratory of Marine Environmental Corrosion and Bio-fouling, Institute of Oceanology, Chinese Academy of Sciences, Qingdao 266071, P.R. China. E-mail: zhangdun@qdio.ac.cn; Fax/Tel: +86 532 82898960

† Electronic Supplementary Information (ESI) available: [FT-IR spectra, pH variation of the reaction solution during the hydrothermal process and the tensile strength-strain curves for the C-LDH/CMC bionanocomposite films with different C-LDHs mass contents]. See DOI: 10.1039/x0xx00000x

1. M. Darder, P. Aranda and E. Ruiz-Hitzky, *Adv. Mater.*, 2007, **19**, 1309-1319.
2. H. B. Yao, H. Y. Fang, Z. H. Tan, L. H. Wu and S. H. Yu, *Angew. Chem. Int. Ed.*, 2010, **49**, 2140-2145.
3. H. B. Yao, Z. H. Tan, H. Y. Fang and S. H. Yu, *Angew. Chem. Int. Ed.*, 2010, **49**, 10127-10131.
4. L. J. Bonderer, A. R. Studart and L. J. Gauckler, *Science*, 2008, **319**, 1069-1073.
5. M. Kumar, R. A. A. Muzzarelli, C. Muzzarelli, H. Sashiwa and A. J. Domb, *Chem. Rev.*, 2004, **104**, 6017-6084.
6. A. M. Fogg, V. M. Green, H. G. Harvey and D. O'Hare, *Adv. Mater.*, 1999, **11**, 1466-1469.
7. S. O'Leary, D. O'Hare and G. Seeley, *Chem. Commun.*, 2002, 1506-1507.
8. F. Li and X. Duan, *Struct. Bond.*, 2006, **119**, 193-223.
9. Z. Y. Tang, N. A. Kotov, S. Magonov and B. Ozturk, *Nat. Mater.*, 2003, **2**, 413-U418.
10. P. Podsiadlo, A. K. Kaushik, E. M. Arruda, A. M. Waas, B. S. Shim, J. Xu, H. Nandivada, B. G. Pumplun, J. Lahann, A. Ramamoorthy and N. A. Kotov, *Science*, 2007, **318**, 80-83.
11. S. Deville, E. Saiz, R. K. Nalla and A. P. Tomsia, *Science*, 2006, **311**, 515-518.
12. E. Munch, M. E. Launey, D. H. Alsem, E. Saiz, A. P. Tomsia and R. O. Ritchie, *Science*, 2008, **322**, 1516-1520.
13. J. F. Wang, L. Lin, Q. F. Cheng and L. Jiang, *Angew. Chem. Int. Ed.*, 2012, **51**, 4676-4680.
14. W. F. Lee and Y. C. Chen, *Eur. Polym. J.*, 2006, **42**, 1634-1642.
15. W. F. Lee and Y. C. Chen, *J. Appl. Polym. Sci.*, 2005, **98**, 1572-1580.
16. J. H. Choy, S. Y. Kwak, J. S. Park, Y. J. Jeong and J. Portier, *J. Am. Chem. Soc.*, 1999, **121**, 1399-1400.
17. M. Darder, M. Lopez-Blanco, P. Aranda, F. Leroux and E. Ruiz-Hitzky, *Chem. Mater.*, 2005, **17**, 1969-1977.
18. L. Y. Chen, Z. G. Tian and Y. M. Du, *Biomaterials*, 2004, **25**, 3725-3732.
19. S. C. Chen, Y. C. Wu, F. L. Mi, Y. H. Lin, L. C. Yu and H. W. Sung, *J. Control. Release*, 2004, **96**, 285-300.
20. Y. H. Lin, H. F. Liang, C. K. Chung, M. C. Chen and H. W. Sung, *Biomaterials*, 2005, **26**, 2105-2113.
21. Q. Xu, C. Mao, N. N. Liu, J. J. Zhu and J. Sheng, *Biosens. Bioelectron.*, 2006, **22**, 768-773.
22. N. A. Mohamed and N. A. Abd El-Ghany, *Cellulose*, 2012, **19**, 1879-1891.
23. S. H. Yu, S. J. Wu, D. W. Tang, Y. C. Ho, F. L. Mi, T. H. Kuo and H. W. Sung, *Carbohydr. Polym.*, 2012, **87**, 531-536.
24. G. H. Yang, J. T. Cao, L. L. Li, R. K. Rana and J. J. Zhu, *Carbon*, 2013, **51**, 124-133.
25. R. L. Patale and V. B. Patravale, *Carbohydr. Polym.*, 2011, **85**, 105-110.
26. H. Wang, C. Zheng and F. Li, *Chem. Eng. J.*, 2010, **158**, 633-640.
27. R. Xu, W. Pang and Q. Huo, *Modern Inorganic Synthetic Chemistry*, Elsevier, 2011.
28. D. G. Evans and R. C. T. Slade, *Struct. Bond.*, 2006, **119**, 1-87.
29. L. Y. Wang, C. Li, M. Liu, D. G. Evans and X. Duan, *Chem. Commun.*, 2007, 123-125.
30. S. S. Vaghani, M. M. Patel and C. S. Satish, *Carbohydr. Res.*, 2012, **347**, 76-82.
31. J. F. Li, J. Yao, Y. M. Li and Y. Shao, *J. Environ. Sci. Health Part B-Pestic. Contam. Agric. Wastes*, 2012, **47**, 795-803.
32. M. L. Duarte, M. C. Ferreira, M. R. Marvao and J. Rocha, *Int. J. Biol. Macromol.*, 2002, **31**, 1-8.
33. S. B. Zeng, X. L. Xu, S. K. Wang, Q. K. Gong, R. J. Liu and Y. Yu, *Mater. Chem. Phys.*, 2013, **140**, 159-167.
34. W. H. Huang, X. Dou and P. Jiang, in *Bioinspiration, Biomimetics, and Bioreplication*, eds. R. J. MartinPalma and A. Lakhtakia, 2011.
35. S. L. Sun and A. Q. Wang, *J. Hazard. Mater.*, 2006, **131**, 103-111.
36. J. Song, *Journal of Qingdao Agricultural University (Natural Science)*, 2009, **26**, 160-162 (in Chinese).
37. Q. Sun, J. Wen and J. Fu, *Advances in Fine Petrochemicals*, 2009, **10**, 45-47 (in Chinese).
38. H. Wang, G. L. Fan, C. Zheng, X. Xiang and F. Li, *Ind. Eng. Chem. Res.*, 2010, **49**, 2759-2767.
39. U. Costantino, F. Marmottini, M. Nocchetti and R. Vivani, *Eur. J. Inorg. Chem.*, 1998, 1439-1446.
40. M. Adachi-Pagano, C. Forano and J. P. Besse, *J. Mater. Chem.*, 2003, **13**, 1988-1993.
41. M. Ogawa and H. Kaiho, *Langmuir*, 2002, **18**, 4240-4242.
42. W. H. R. Shaw and J. J. Bordeaux, *J. Am. Chem. Soc.*, 1955, **77**, 4729-4733.
43. Y. Wang, D. Zhang, Q. Bao, J. J. Wu and Y. Wan, *J. Mater. Chem.*, 2012, **22**, 23106-23113.
44. A. M. Raichur, *J. Dispersion Sci. Technol.*, 2007, **28**, 1272-1277.
45. B. M. Cerrutti, J. C. Lamas, S. P. Campana and E. Frollini, *J. Polym. Environ.*, 2013, **21**, 816-825.
46. F. L. Mi, H. F. Liang, Y. C. Wu, Y. S. Lin, T. F. Yang and H. W. Sung, *J. Biomater. Sci.-Polym. Ed.*, 2005, **16**, 1333-1345.
47. N. A. Gujarathi, B. R. Rane and J. K. Patel, *Int. J. Pharm.*, 2012, **436**, 418-425.
48. Y. Wang and D. Zhang, *Surf. Coat. Technol.*, 2012, **210**, 71-77.
49. Y. T. Zhang, L. H. Fan, T. T. Zhi, L. Zhang, H. Huang and H. L. Chen, *J. Polym. Sci., Part A: Polym. Chem.*, 2009, **47**, 3232-3240.



## Graphic Abstract

